Biomicrofluidics ARTICLE scitation.org/journal/bmf

Continuous electrical lysis of cancer cells in a microfluidic device with passivated interdigitated electrodes

Cite as: Biomicrofluidics 14, 064101 (2020); doi: 10.1063/5.0026046
Submitted: 20 August 2020 · Accepted: 17 October 2020 ·
Published Online: 2 November 2020

K. Pandian, M. Ajanth Praveen, S. Z. Hoque, A. Sudeepthi, and A. K. Sen[a)]

AFFILIATIONS

Micro Nano Bio–Fluidics Unit, Fluid Systems Laboratory, Department of Mechanical Engineering, Indian Institute of Technology Madras, Chennai 600036, India

[a)]**Author to whom correspondence should be addressed:** ashis@iitm.ac.in

ABSTRACT

Cell lysis is a critical step in genomics for the extraction of cellular components of downstream assays. Electrical lysis (EL) offers key advantages in terms of speed and non-interference. Here, we report a simple, chemical-free, and automated technique based on a microfluidic device with passivated interdigitated electrodes with DC fields for continuous EL of cancer cells. We show that the critical problems in EL, bubble formation and electrode erosion that occur at high electric fields, can be circumvented by passivating the electrodes with a thin layer ($\sim$18 μm) of polydimethylsiloxane. We present a numerical model for the prediction of the transmembrane potential (TMP) at different coating thicknesses and voltages to verify the critical TMP criterion for EL. Our simulations showed that the passivation layer results in a uniform electric field in the electrode region and offers a TMP in the range of 5–7 V at an applied voltage of 800 V, which is well above the critical TMP ($\sim$1 V) required for EL. Experiments revealed that lysis efficiency increases with an increase in the electric field (E) and residence time (t_r): a minimum $E \sim 10^5$ V/m and $t_r \sim 1.0$ s are required for efficient lysis. EL of cancer cells is demonstrated and characterized using immunochemical staining and compared with chemical lysis. The lysis efficiency is found to be $\sim$98% at $E = 4 \times 10^5$ V/m and $t_r = 0.72$ s. The efficient recovery of genomic DNA via EL is demonstrated using agarose gel electrophoresis, proving the suitability of our method for integration with downstream on-chip assays.

I. INTRODUCTION

Understanding the behavior of cells during a disease condition and the way it processes information and acquires specific characters among the whole population is one of the critical challenges in the field of cell biology.[1] Cell heterogeneity is an important clue for a better understanding of the causes and progression of diseases such as cancer.[2,3] Intracellular components enabling information about genetic and disease characteristics are the fundamental elements for medical diagnostics. Cell lysis is a critical step in cell-based assays, which enables access to the cellular components by disrupting the integral and complex membranous structure and facilitates profiling the intracellular components such as DNA, RNA, and protein. The membrane wound around a cell, composed of a lipid bilayer with various proteins embedded in it, has a basic function of separating the interior of the cell from the external environment. The topology and chemistry of the extracellular membrane act as a barrier that controls the movement of substances across the cell through selective permeabilization of ions and organic molecules. Lysing a cell without damaging its genetic components is a challenging task, and it can be achieved either by denaturing or destabilizing the membrane components (via chemical or thermal means) or by disrupting the bonds between the membrane via electrical,[4–6] mechanical,[7] and acoustic[8] methods. The additional purification step incorporated in the chemical lysis, inactivation steps in enzyme assisted lysis, and extra dilutions for detergent-based lysis limits their utility in the on-chip analysis.[9] The lytic reagents, namely, detergents, chaotropic salts, enzymes, and alkaline may interfere with subsequent molecular assays.[10] Denaturation of proteins and other biological matters is of concern in the case of the thermal lysis method. Bubbles generated via acoustic waves were used to rupture lipid membranes by the simple

oscillation mechanism,[11] and high throughput cell lysis was achieved by actuating sound waves on the cell surface without damaging its genetic components.[12] However, the open surface cell treatment is unsafe and accessible for easy contamination. Electrical lysis (EL) associated with irreversible electroporation is a promising technique to prepare samples for genetic analysis due to its purely physical nature and fast and simple operation.[13–16] Chemical-free cell lysis methods such as induced rapid electric pulses and the genetic material capture by magnetic beads also gained attention because of high throughput.[17,18]

Electrical lysis (EL) is the process of breaking the cell membrane by exposing it to a high electric field to release the intracellular components. Compared to conventional methods, the microfluidic chip-based cellular genetic analysis offers various advantages such as the low reagent volume, high surface-to-volume ratio, low cost, and easy handling for cell analysis.[19] Though the electrical cell lysis technique existed for several years, it has generated much interest recently due to the noteworthy advantages of on-chip EL to recuperate the genetic materials without any damage and contamination.[20] Generating an electric field inside a microchannel is of greater advantage, which includes low current requirements and effective utilization of energy.[21] On-chip EL has unique features such as rapid operation, low power, low cost, controllability, automation, and on-chip integration for continuous downstream analysis avoiding contamination and easy implementation. The major requirements for a device to perform cell lysis effectively include speed (to prevent further biochemical changes), selectivity (breaking down cell membranes while protecting organelle membranes), and integration with devices for downstream analysis,[22] which can potentially be achieved by performing continuous electrical lysis in a microfluidic device, which is the focus of the present work.

A microfluidic electroporation device with a superior geometric design was developed that selectively lysed the cell plasma membrane and left the organelle membrane undamaged, although the lysis efficiency was found to be low due to incomplete cell lysis.[23] Electrical cell lysis following cell trapping inside an array of microwells was found to be efficient, although the loss of cells during trapping before lysis remained an issue.[24] A microchamber comprising an array of nano-spikes, which required a complex fabrication procedure, was used for low-voltage AC lysis.[25] Carbon electrode pillars were employed in a microchannel device for the efficient lysis of yeast cells in osmotically balanced solutions;[26] however, device fabrication was very challenging. Furthermore, bubbles were observed at higher voltages, and the lysis efficiency was found to be small. An electrochemical technique involving the alkaline solution was also demonstrated for cell lysis,[27] but it involved the use of chemicals that may not be compatible with downstream analysis. An array of carbon nanotubes (CNTs) was utilized in a microfluidic device for the lysis of *E. coli*, although it involved a complicated fabrication technique and device architecture.[28] Recently, a simple and promising device design for the lysis of human blood cells offering excellent lysis efficiency was reported.[29] However, the literature indicates that human blood cells are relatively easier to lyse compared to circulating tumor cells (CTCs) due to the complexity of the cell membrane in cancer cells.[29,30] We see that there is a need to develop an efficient CTC lysis method that is simple in terms of fabrication and handling and can facilitate continuous lysis of CTCs and is proven to be compatible with downstream analysis. In the present work, we report a simple and easy-to-fabricate microfluidic device, demonstrate continuous lysis of different types of CTCs, and show the potential application of the lysis technique for downstream analysis.

The fundamental requirement for achieving cell lysis through electrical discharge is the transmembrane potential (TMP)—a difference in the electric potential between the interior and the exterior of a cell membrane.[31] Conversely, experimental studies demonstrated that merely exceeding the threshold potential could lead to reversible electroporation and advocate higher voltages as prerequisites for effective disruption of the cell membrane.[15] Both direct current (DC) and alternating current (AC) sources can be used for electrical cell lysis. An AC field can minimize water electrolysis and Joule heating problems but generates a discontinuous electric field and thereby may lead to reversible electroporation and inappropriate lysis resulting in poor lysis efficiency, and it may not be applicable to a wide range of cell types.[26] If the electric field pulse width is shorter than a critical time (relaxation time), which may again depend on the cell type, the pores will be unstable and disappear as in the case of electroporation.[32] Typically, a high DC field is an ideal choice for cell lysis through electroporation as it makes the cell membrane experience a higher TMP continuously and leads to irreversible electroporation without affecting the subcellular organelles.[21,23,33] In the case of a DC field, with a persistent electric field, the pores are stable and undergo molecular rearrangement resulting in efficient cell lysis.[32] Furthermore, the application of continuous DC voltage greatly simplified the instrumentation compared to the setup required for electrical pulses/AC voltages.[30] However, a high DC field offering efficient cell lysis may eventually exceed the water electrolysis threshold and would inevitably lead to the formation of bubbles and erosion of electrodes even in microscale devices.[26,31,34]

Here, we demonstrate continuous electrical lysis of cancer cell lines in a microfluidic device integrated with passivated interdigitated electrodes. We employ a higher DC field (~100–800 V) to achieve excellent lysis efficiency while addressing electrolysis and Joule heating problems by coating the electrodes with a thin layer of poly dimethyl siloxane (PDMS) as the dielectric material. We performed numerical simulations to determine the TMP at different coating thicknesses and applied voltages and experiments to study the effect of applied voltage and residence time (flow rate) on the lysis efficiency. Cell lysis of four different cancer cell lines, cervical cancer cell line (HeLa), prostate cancer cell line (DU 145), and breast cancer cell lines (MDA MB 231, and MCF 7), is demonstrated. To prove the suitability of the technique for downstream analysis, the cellular DNA concentration is analyzed using agarose gel electrophoresis.

II. EXPERIMENTAL

A. Device description and electrical lysis mechanism

The device [Fig. 1(a)] comprises a straight microchannel of width $W = 60\,\mu m$, depth $h = 50\,\mu m$, and an array of interdigitated electrodes patterned on the bottom surface of the channel. The spacing between adjacent electrodes is $s = 40\,\mu m$ and the electrode

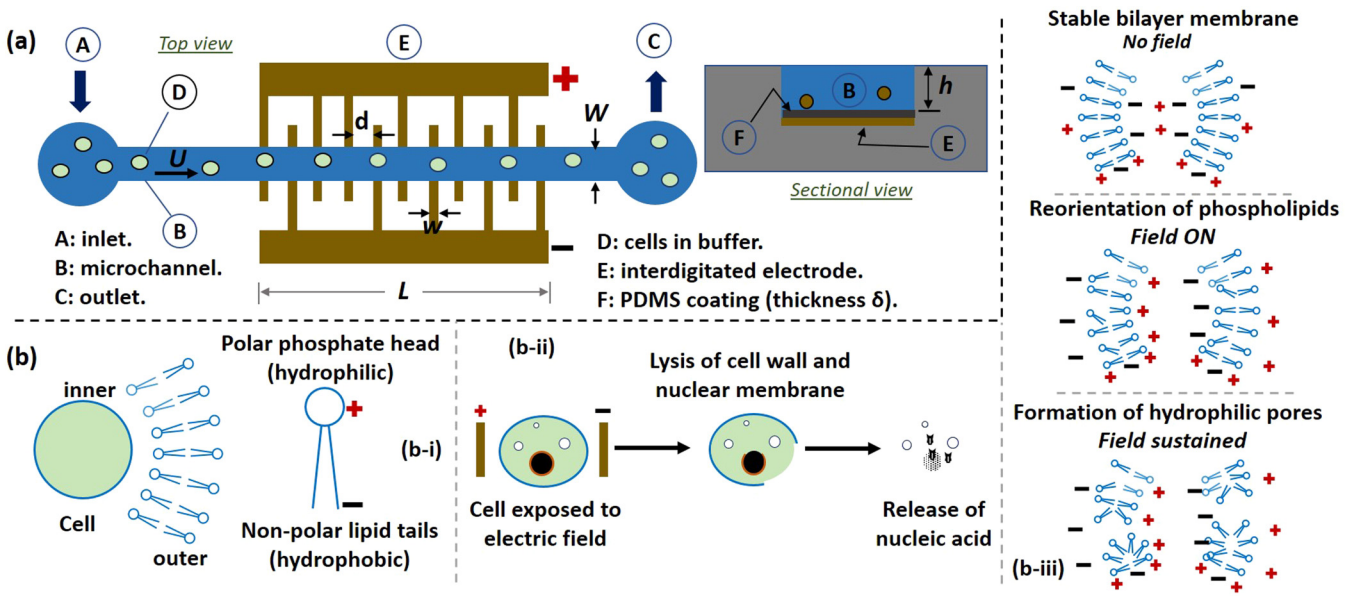

FIG. 1. (a) Schematic of the on-chip continuous EL device: the top view shows the microchannel and interdigitated electrodes and the cross-sectional view shows PDMS coating on electrodes. (b) Schematic of (i) cell structure, (ii) EL process: EL of the cell wall, nuclear membrane, release of nucleic acid, and (iii) modification of the membrane bilayer during EL.

thickness is w = 60 μm; there are N = 12 pairs of electrodes and the overall length of the electrode region is L = 1.2 mm. Consequently, the residence time of the cells flowing in the channel at a velocity U (or a flow rate Q) will be t_r = (L/U) = (WhL/Q). The electrodes are coated with a thin layer of PDMS of thickness δ, which isolates the electrodes from the sample flowing in the channel and thus prevents the formation of bubbles and erosion of electrodes. The bubbles may form at the electrodes due to ionic nature (high electrical conductivity) of the sample,[21,35,36] that may alter the cell pH, causing damage to the cell DNA.[37] Furthermore, the exposure of electrodes to ionic liquid under a high electric field may trigger chemical reactions at the electrode leading to joule heating and erosion of electrodes. We circumvented the above issues by passivating the electrodes with a layer of PDMS, as discussed later.

The structure of a cell and electrical lysis (EL) mechanism is shown in Fig. 1(b). The cell wall comprises a sheet of phospholipid molecules having polar phosphate head (hydrophilic) and non-polar lipid tails (hydrophobic) arranged in a bilayer formation [Fig. 1(b-i)]. When a cell is exposed to an external electric potential greater than the transmembrane potential (TMP), the bilayer gets ruptured and subsequently, the nuclear membrane opens up releasing the nucleic acid [Fig. 1(b-ii)]. Although the exact dynamics involved in a rupture of the membrane is still debated, the current understanding points toward the formation of pores attributed to the reorientation of the phospholipid molecules.[38] Exposure of a cell suspended in an ionic fluid to a high electric field leads to an accumulation of charges on both sides of a cell membrane, resulting in an induced transmembrane potential across the cell membrane [Fig. 1(b-iii)]. If the electric field is high enough such that the transmembrane potential exceeds a critical value (~1.0 V), the phospholipid molecules undergo conformal changes causing a large number of hydrophilic pores through the cell membrane. If the electric field is taken off before a critical time (relaxation time), the pores are unstable and disappear as in the case of electroporation but with a persistent electric field (~10^5 V/m), the pores are stable and undergo molecular rearrangement to form nanometer-sized pores (~40 nm), a phenomenon is known as electrical lysis.[32]

B. Materials and methods

Human cancer cell lines: HeLa, DU 145, MDA MB 231, and MCF 7 cells were cultured. The cells were serially passaged as monolayer cultures in the DMEM medium (Himedia, Mumbai, India) supplemented with 10% fetal bovine serum (FBS, Himedia) and 1% antimycotic antibiotic solution (Himedia). The cell culture dish was incubated in a humidified atmosphere containing 5% carbon dioxide at 37 °C. Cells grown to sub-confluence were washed with phosphate-buffered saline (PBS, Himedia, pH 7.4) and harvested by a 5 min treatment with 0.25% Trypsin EDTA (ethylenediamine tetraacetic acid). The cell pellet was collected by centrifugation at 1500 rpm for 6 min. Finally, the cells were suspended in a working solution of the cell medium before the experiments. To match the density of cells and to avoid settlement of cells at the device inlet, 18% of optiprep (Sigma Aldrich, India) was added to the working solution. For chemical lysis, cells were suspended in a lysis buffer (100 mM Tris pH 8.0, 2% Tween-20,

proteinase K 1.5 μg/μl; Sigma Aldrich, Germany) followed by incubation in a water bath at 55 °C for 15 min. The lysis mixture was then heated at 90 °C for 2 min for enzyme inactivation. Cell pellets were collected by centrifugation and then microscopic imaging was carried out. Both in electrical and chemical lysis, cell lysis efficiency was calculated by image analysis using trypan blue (Himedia, Mumbai, India) assay, where the outlet cell solution is loaded with 1:1 of trypan blue dye to check the dead/lysed cells. To demonstrate the downstream utility of the proposed electrical lysis method, DNA purification and gel electrophoresis were performed. Crude cell lysate from the device outlet was collected and diluted with 1× Tris EDTA buffer (Sigma Aldrich, Mumbai, India) and centrifuged at 1500 rpm for 7 min. The cell pellet was purified using an QIA quick DNA Purification kit (QIAGEN, Germany). The purified DNA sample is loaded in 1% agarose gel, and the sample concentration was compared by running 1 kb gene ruler DNA ladder (Thermo Scientific, India).

C. Device fabrication and experimental setup

The device was fabricated by first preparing the patterned electrode layer and coating the electrodes with PDMS, and then bonding with a PDMS microchannel layer. The patterned electrode layer (chromium and gold films, Cr/Au: 30 nm/100 nm) was fabricated by using electron-beam evaporation and photolithography followed by etching. A detailed fabrication procedure is outlined in Sec. S1 of the supplementary material. Subsequently, a thin layer of PDMS mixed with *n*-hexane[39] was coated on the patterned electrode layer and cured. The %n-hexane, coating speed, and time duration used for coating the PDMS layer are discussed in Sec. IV A. The microchannel was fabricated in a poly dimethyl siloxane (PDMS) material by first preparing a silicon-SU8 master using photolithography and then using soft lithography.[40] The microchannel and PDMS-coated patterned electrode layers were exposed to oxygen plasma (PDC-002, Harrick Plasma, USA) at 30 W power for 2 min and bonded together to obtain the microfluidic device. A schematic and a photograph of the experimental setup are shown in Figs. 2(a) and 2(b), respectively. The cell sample was infused into the device using a high-performance syringe pump (Cetoni, Germany) from a 1.0 ml glass syringe. The sample flow rate was varied in the range of 0.3–1 μl/min. The electrodes were energized with a DC high voltage power supply (SRS Sandford research systems). The DC voltage was varied in the range of 100–800 V. The lysed sample from the outlet was collected in 1× TE buffer in an Eppendorf tube for further analysis. The fluidic connection between the syringe pump and the device inlet and between the device outlet and the Eppendorf tube was established using PE tubing (Instech Laboratories, USA).

III. NUMERICAL MODEL

Numerical simulations are carried out using COMSOL Multiphysics 5.4 to simulate the potential and electric field in the electrode region and find the TMP across a cell as it crosses the electrode region. The governing equations used for solving the potential and electric field are given as follows:,[41]

$$\nabla \cdot J = 0, \tag{1}$$

$$J = \sigma E + J_e, \tag{2}$$

$$E = -\nabla V, \tag{3}$$

where E represents the electric field due to applied voltage V, σ is the electrical conductivity, J is the current density, and J_e is the external current density. A schematic of the simulation domain is shown in Fig. 3. Electric potential and ground boundary conditions are used on the electrodes, and electric insulation boundary condition is used on the channel walls and PDMS coating. Since the mammalian cell membrane is very thin (typically ∼nm), it is extremely challenging to directly model such a thin membrane structure around a cell. Herein, the membrane is explicitly modeled by enforcing a boundary condition that satisfies the continuity of

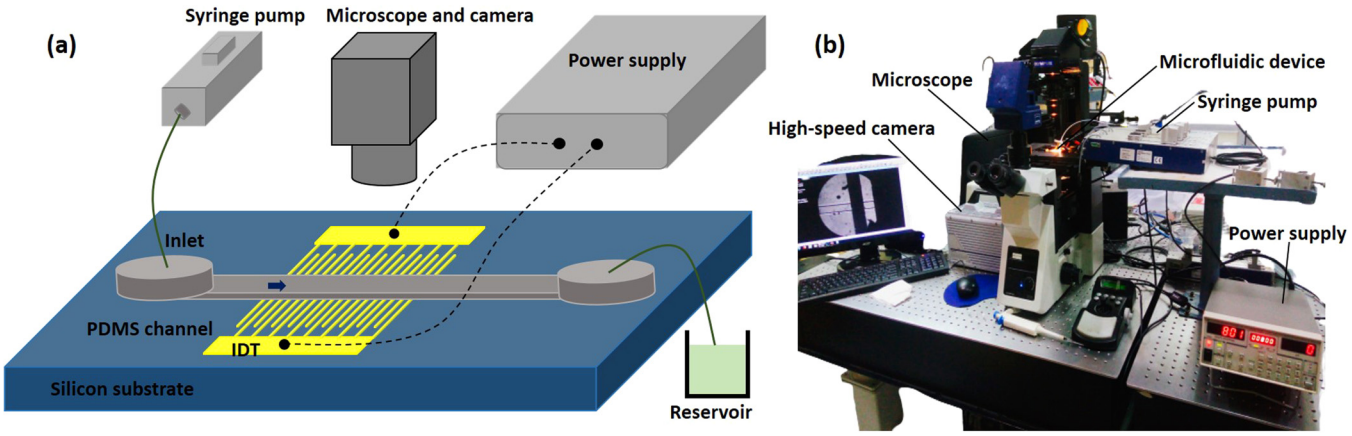

FIG. 2. (a) Schematic and (b) photograph of the experimental setup used for the continuous cell lysis experiments.

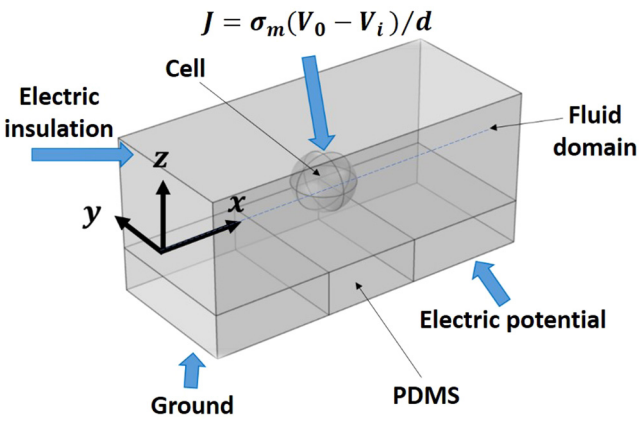

FIG. 3. Schematic of the simulation domain, with a 25 μm spherical cell placed inside the fluid domain, located at the center of an adjacent pair of electrodes and middle of the channel depth.

the electric current density across the membrane is asfollows:[42,43]

$$J = \sigma_m(V_0 - V_i)/d, \tag{4}$$

where σ_m is the electrical conductivity of the membrane, d is the membrane thickness, and V_0 and V_i are the electric potentials at the outer and inner sides of the membrane, respectively. The simulation parameters such as the different material properties (permittivity and conductivity) of the cell cytoplasm and the ratio of membrane conductivity to thickness are listed in Table I. Typically, the simulation domain is divided into five different regions, viz., ground, electrical potential, PDMS layer, cell, and fluid region. Physics controlled extra-fine meshing is carried out in all the regions to accurately evaluate the TMP values from the simulations. The mesh generated for the 3D steady-state simulation consists of 84 484 elements with average element quality of 0.66. There were 6580, 456, and 26 numbers of triangular, edge, and vertex elements, respectively. Equations (1)–(4) were solved to obtain the transmembrane potential and electric field distribution across the cell wall, as described in Sec. IV.

IV. RESULTS AND DISCUSSIONS

A. Electrode passivation and transmembrane potential

Electrodes were passivated with a layer of PDMS to prevent electrode erosion and bubble formation. With 10% *n*-hexane and 4000 rpm for 60 s, the thickness of the PDMS layer measured using scanning electron microscopy (SEM) was found to be 18 μm [Fig. 4(a)]. The variation of the PDMS coating thickness with % of *n*-hexane and the spin coating speed is shown in Fig. 4(b). With smaller %n-hexane, the PDMS coating was thicker (>18 μm) and non-uniform even at higher speeds [Fig. 4(c)]. A thicker PDMS layer prevents cell lysis even at higher voltages [Fig. 4(d)]. For a higher %n-hexane, the thickness of the PDMS layer was found to be smaller (<18 μm) and, therefore, erosion of electrodes was observed even with a voltage as low as 10 V. Therefore, we proceed with a passivation layer thickness of 18 μm.

Experiments were performed with devices with and without the PDMS coating on the electrodes. In both cases, the microchannel was filled with PBS buffer used for suspending cells. Without a PDMS coating, when the electrodes were energized even with a voltage as low as 10 V, we observed bubble formation (electrolysis) and electrode erosion within 5 min of the start of operation [Fig. 5(a)]. However, in the device with a PDMS coating (18 μm), even with a voltage as high as 800 V, the formation of bubbles or erosion of electrodes was not observed even after several hours (>2 h) [Fig. 5(b)]. At 10 V, the electric field is ~10^5 V/m, and without the PDMS coating, such electric fields can cause electrolysis in an ionic sample leading to gas bubble formation.[35,36] Besides, the Joule heating effect at the electrodes also contributes to the bubble formation.[21] The size of the bubbles formed was found to be proportional to the voltage applied [Fig. 5(c)]. The bubbles thus formed will interfere not only with the cell lysis process but also with the intracellular elements such as the extracted nucleic acids for downstream analysis and measurements. The handling of bubbles and their removal is a critical challenge in microfluidics[46] and thus need to be avoided. Furthermore, electrochemical reactions at the electrodes resulting in the formation of ions of PBS lead to the erosion of electrodes forming metal hydroxides.[47] Besides electrochemical reactions, the generation of tinier of bubbles at the electrodes could lead to pitting by cavitation and erosion of electrodes. Without passivation, at a DC voltage of 10 V, the electrodes were degraded within 2–3 min of operation. By passivating the electrode layer with PDMS coating (18 μm thick), first of all, the ionic sample buffer is isolated from the electrode, thereby preventing electrochemical reaction and Joule heating and, therefore, bubble formation. Furthermore, in the absence of electrochemical reactions, the electrode erosion problem is also inhibited. However, PDMS being a dielectric material (of dielectric constant ~2.3–2.8),[48] the effective electric field in the ionic buffer is significantly reduced, requiring a higher voltage to achieve the required TMP, as discussed later. At a DC voltage of 800 V, the electrodes coated with PDMS could be safely operated up to several hours of operation without any sign of degradation.

TABLE I. The values of material properties of different type of cells considered for simulations.

Cell type	The electrical conductivity of cytoplasm, σ_c (S m^{-1})	The relative permittivity of cytoplasm, ε	The ratio of membrane conductivity to thickness, σ_m/d(S m^{-2})	Reference
MCF 7	0.23	78.69	243	44
HeLa	0.15–0.4	45	244	45

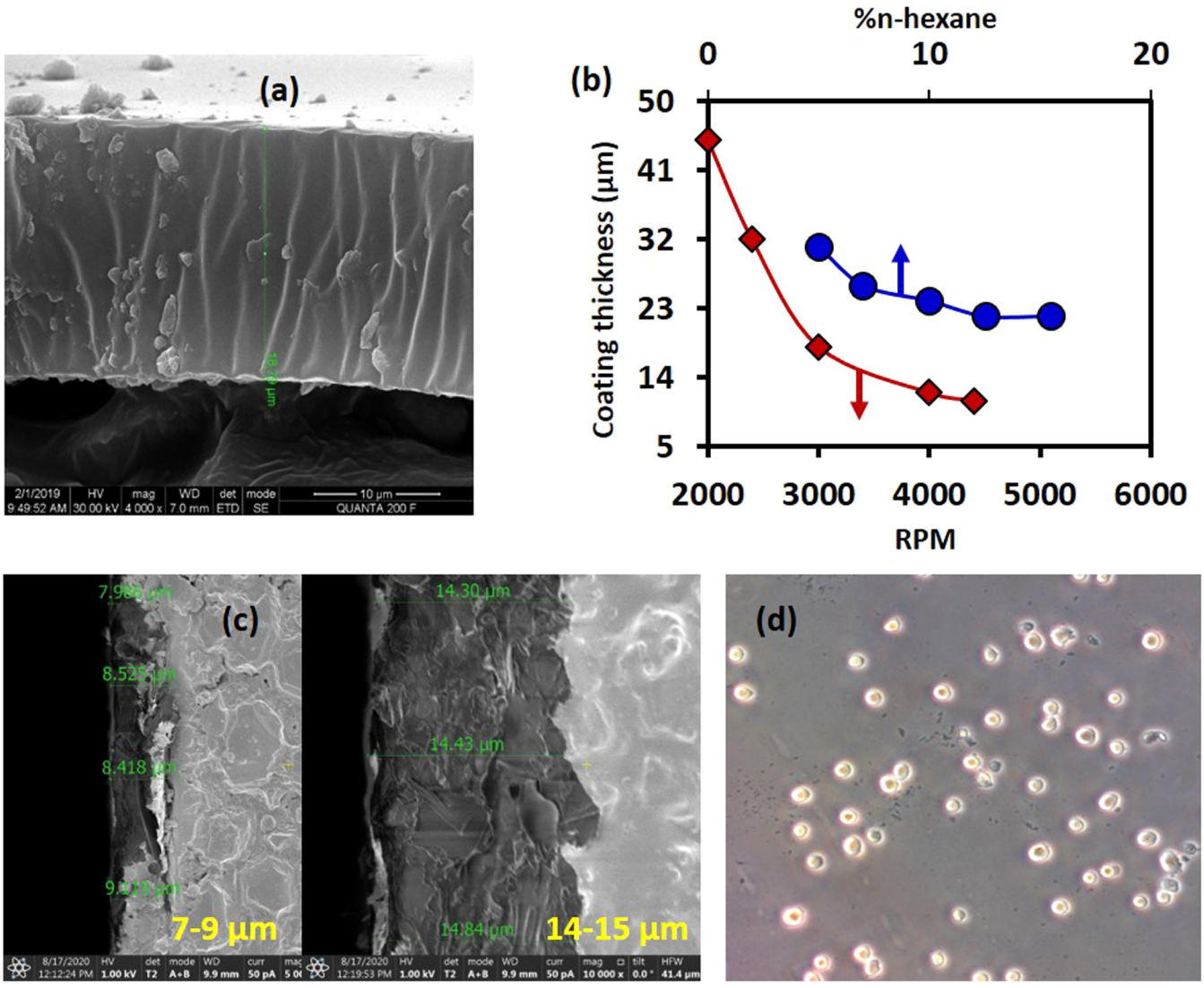

FIG. 4. (a) Scanning electron microscope (SEM) image of the passivation layer with 10% *n*-hexane and 4000 rpm. (b) Variation of PDMS coating (passivation layer) thickness with %*n*-hexane and coating speed. (c) A non-uniform coating of PDMS (in the same glass slide) at a lower percentage of *n*-hexane (5% *n*-hexane) at 4000rpm. (d) The absence of cell lysis (DU 145 cells) even after applying 800 V due to thicker PDMS coating (30 μm).

Numerical simulations were performed using the model described earlier and using the domain shown in Fig. 3. The potential was varied in the range 100–800 V, with the electrical conductivity of the buffer to be 1.6 S/m. The width of the channel is 60 μm, and the thickness of the PDMS coating is varied in the range 0–18 μm. The height of the channel was 50 μm and 68 μm, respectively, with or without the PDMS coating. In devices with and without a PDMS layer, at a voltage of 100 V, the electric potential and electric field contours across an x–y plane passing through the center of the channel are presented in Fig. 6. The maximum potential is smaller with a 18 μm thick PDMS layer (51 V) as compared to that without the PDMS layer (80 V). The maximum electric field with the PDMS layer ($\sim 10^4$ V/m) is found to be one order of magnitude smaller compared to the case without the layer ($\sim 10^5$ V/m) due to the dielectric nature of the PDMS coating.

Typically, the electric field is highly non-uniform above the electrode arrays with sharp spikes near the edges of the electrodes, as reported in the literature.[29,49] We have plotted the variation of the electric potential and the electric field between the electrodes at three different z-positions, z = 0, 10, and 30 μm for both with and without considering the PDMS (passivation) layer of thickness

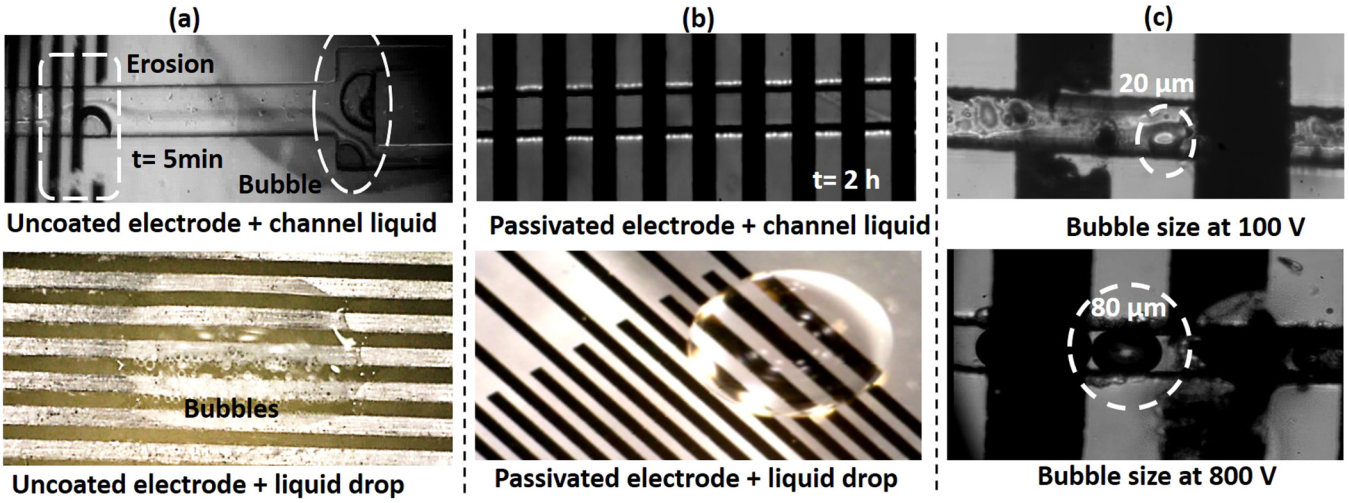

FIG. 5. Experimental images showing (a) bubble formation and electrode erosion of electrodes without PDMS coating, voltage 10 V, within 5 min. (b) Bubble formation and electrode erosion inhibited with PDMS coating of thickness 18 μm, 800 V, even after 2 h. (c) The size of bubbles increases (approximately four times) with an increase in voltage, 100 V and 800 V, at 10 min.

18 μm, as shown in Fig. 7. The adjacent edges of the pair of electrodes are at the locations x = 50 μm and x = 90 μm, and the gap between the electrode is 40 μm, which is the same as that used in the experiments. In the present case, with a PDMS layer of 18 μm thickness, our simulations show the sharp peaks near the electrode edges, at z = 0, which is the bottom of the PDMS layer (or the top of the electrodes) [see Fig. 7(b)]. However, we find that the sharp peaks disappear and the non-uniformity in the electric field diminishes as we gradually move away from the electrodes in the z-direction (depth-wise). As observed in Fig. 7(b), the sharp peaks disappear even at z = 10 μm (which is inside the PDMS layer) and at z = 30 μm (in the channel region), the electric field ($\sim 10^5$ V/m) is more uniform compared to the case without a PDMS passivation layer [Fig. 7(c)]. Our simulation results also show a nearly constant value of electric potential ~390 V in the channel (at z = 30 μm). So, we find that the passivation layer gives rise to a more uniform electric potential and electric field in the entire channel region over the electrodes compared to the bare electrode case (without the passivation layer).

The variation of TMP across a cell of 25 μm diameter located at the center of the channel and the electrodes with applied voltage for different PDMS coating thickness is presented in Fig. 7(d). The TMP in the case of the PDMS-coated electrodes is found to be two orders of magnitude lower compared to the uncoated electrode case. The TMP at 100 V and thickness 18 μm is found to be ~0.7 V, which may lead to reversible electroporation.[13,33] Furthermore, with the PDMS-coated electrodes, at 100 V, the electric field at the location of the cell is $\sim 10^4$ V/m, whereas the electric field used in the conventional EL is $\sim 10^5$ V/m. So, to compensate for the loss of the electric field due to electrode passivation, a higher voltage needs to be applied. At a voltage of 800 V, the TMP is found to be ~5 V, which is well above the threshold TMP, ensuring complete disintegration of membrane offering efficient cell lysis as discussed later. As compared to a coating thickness of 18 μm, for a smaller thickness (10 μm), even though the TMP is higher, the problems of bubble formation and electrode erosion were observed. PDMS is a porous material (pore size ~1 μm),[50] the ionic buffer may permeate through the thin layer and interface with the electrode causing the above problem. On the other hand, for a thicker layer of PDMS (30 μm), the electric field effect is suppressed and the field in the ionic fluid region is smaller and cell lysis is affected. So, we proceed with a PDMS layer thickness of 18 μm for the subsequent studies.

Furthermore, we have predicted the TMP values from the simulations for two different types of cells (HeLa and MCF7) with their centers placed at different positions away from the electrodes along the z-direction (and located at the mid-plane between the electrodes, i.e., x = 70 μm) and at different positions between the electrodes along the x-direction (at the middle of the channel along the x-direction, i.e., z = 43 μm), as presented in Figs. 8(a) and 8(b), respectively, which shows less than 5% variation of TMP between the different types of cells. With the passivation layer, and the resulting approximately constant (uniform) electric field in the channel region, we also find that the variation of the TMP of a given cell, depending on its position in the x- and z- directions, varies between ~5 and 7 V, which is much higher than the reference critical TMP.

B. Electrical cell lysis in a static condition

We performed EL experiments by dispensing cell sample droplets of volume 10 μl on the PDMS-passivated electrodes (thickness 18 μm) and exposing the cells to electric fields. Cell concentration was measured using a Neubauer cell counter,[51] and the cell

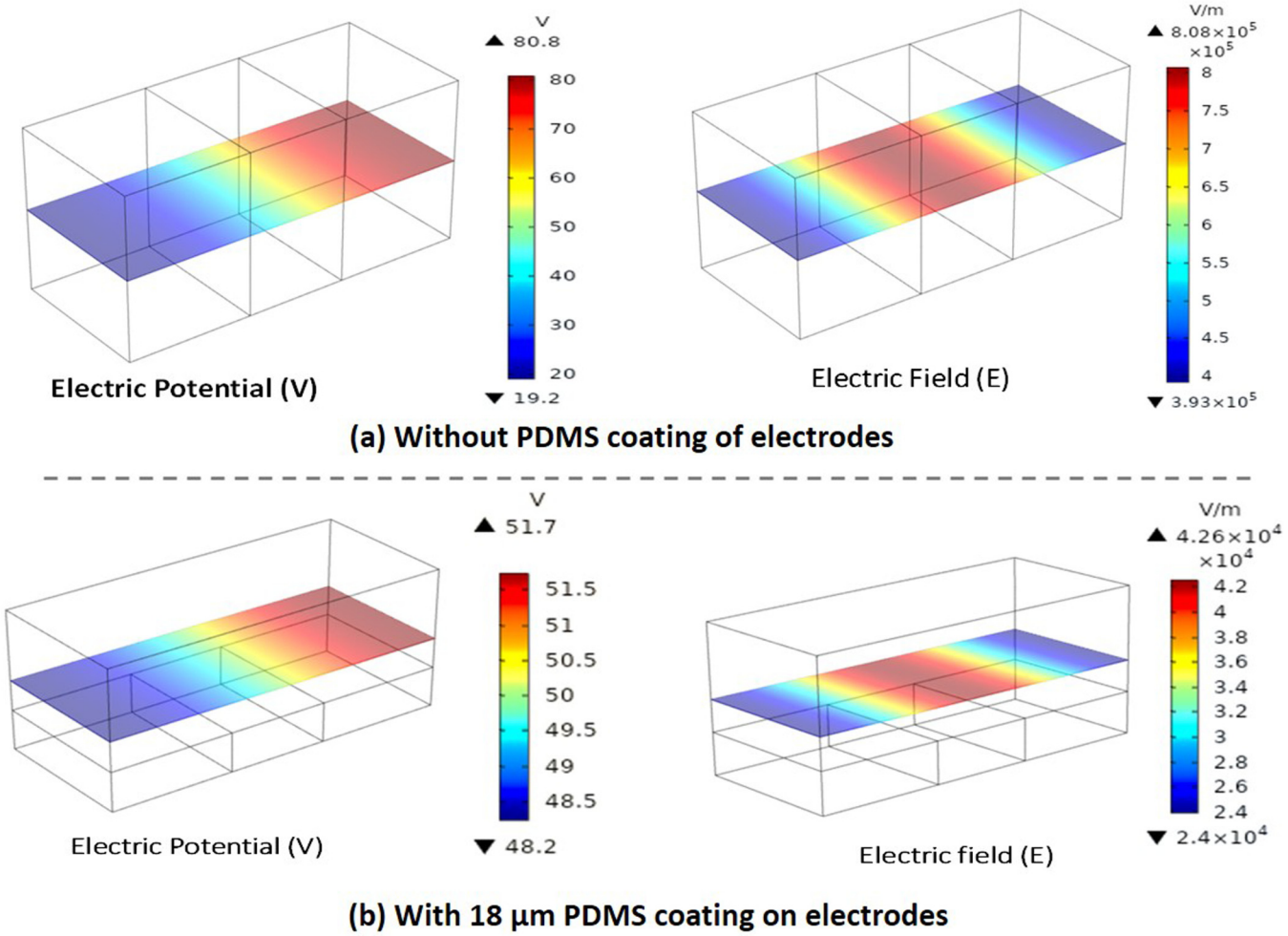

FIG. 6. Simulation results showing the electric potential (V) and electric field (E) distribution inside the domain on an x–y plane across the center of the channel (depth-wise) for a DC voltage of 100 V, (a) without a PDMS layer and (b) with a 18 μm thick PDMS layer.

concentrations were kept fixed as follows: 3×10^4 cells/μl for HeLa cells, 7×10^3 cells/μl for DU 145 cells, 5.3×10^3 cells/μl for MDA MB 231 cells, and 1×10^4 cells/μl for MCF 7. The bright-field microscopic images of the cells after exposing them to 100 V for 0–1 s are presented in Figs. 9(a) and S1 in the supplementary material. As observed, upon the exposure of the cells to the electric field, membrane extrusion and cell enlargement occur [Fig. 9(a-ii)], leading to cell lysis, as per the mechanism illustrated in Sec. II A. The oppositely charged head/tail of phospholipid molecules strongly attract each other resulting in the reorientation of the phospholipid molecules, appearing macroscopically as membrane extrusion and cell enlargement, and give rise to irreversible pore formation thus the membrane becomes permeable to a liquid medium such as trypan blue dye. Furthermore, if the cell continues to get exposed to the high field, the cell membrane disintegrates completely [Fig. 9(a-iii)], releasing the intracellular content. Lysis efficiency was enumerated via trypan blue assay after collecting the lysed sample and the lysis efficiency for all four cell lines was found to be ~90%. To further confirm the cell lysis, in addition to trypan blue assay, which is a dead cell dye, the intensity of the tagged cells with a live cell dye (1× Calcein AM) before and after cell lysis was compared. The confocal microscope image of the DU 145 cells tagged with 1× Calcein AM before [Fig. 9(b-i)] and after [Fig. 9(b-ii)] the electrical lysis shows that the intensity of the cells significantly reduces confirming cell disintegration and lysis.[24]

The EL performance was compared with the conventional chemical lysis method (as control). For chemical lysis, a mixture of proteinase K enzyme, 2% tween 20, and Triton x 100 was used. Upon exposure of the intact cells [Fig. 9(c-i)] to the lysis mixture, a complete disintegration/rupturing of cells was observed [Fig. 9(c-ii)], identical to the final stage of the EL. We demonstrate that our EL method is a suitable alternative to the

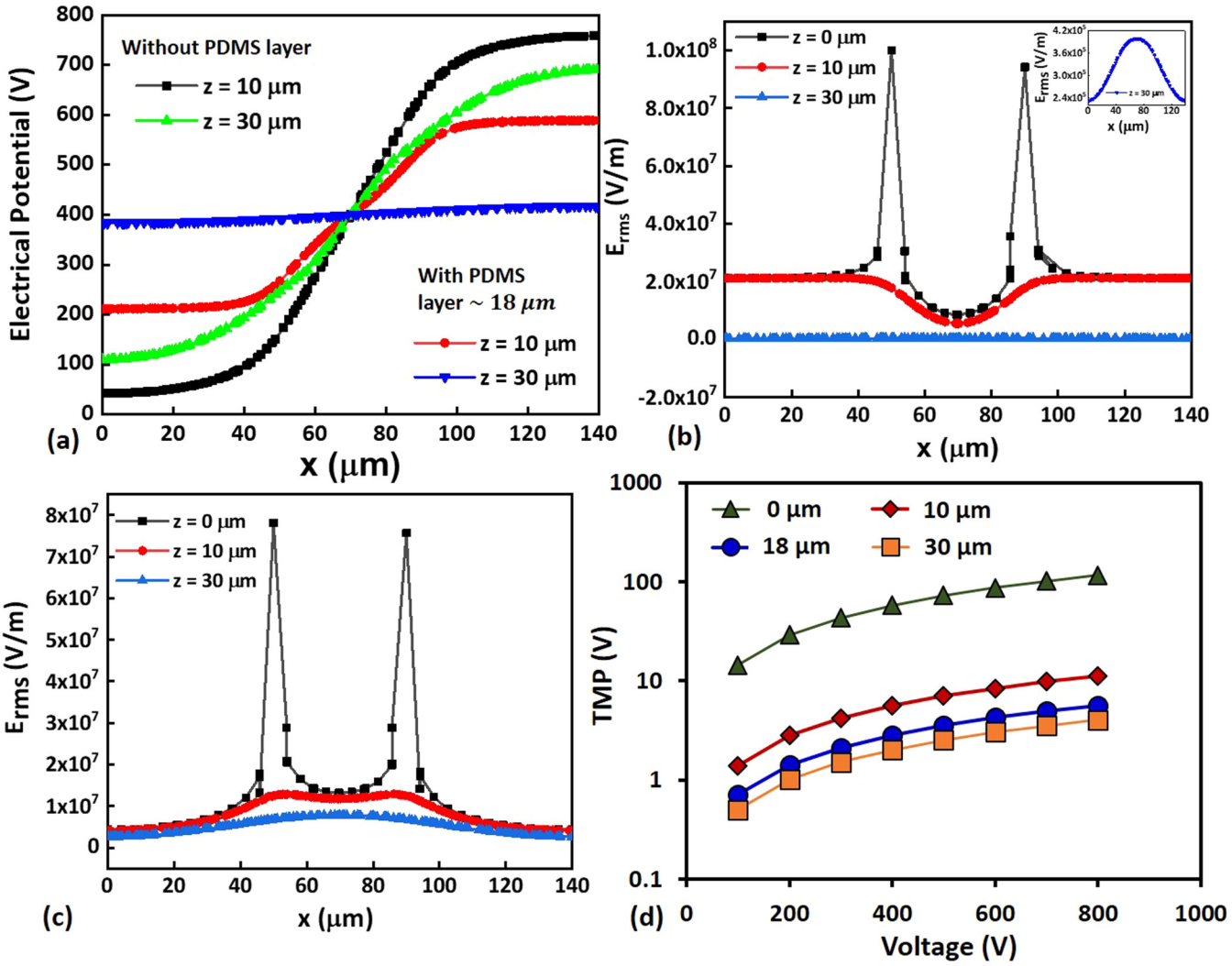

FIG. 7. (a) The variation of the electrical potential along the axial (x-) direction of the microchannel, with a 18 μm PDMS layer and without a PDMS layer. The variation of the electrical field along the axial (x-) direction across electrodes, (b) with 18 μm PDMS layer, the inset shows the variation of the electric field at z = 30 μm along the axial direction, (c) without a PDMS layer. In all cases, applied voltage is 800 V. (d) The variation of TMP across a cell located at the center of the channel and the electrodes with applied voltage, for different values of PDMS coating thickness.

standard chemical-based cell lysis procedures. The gel electrophoresis (GE) results of cellular DNA extracted using EL and the chemical lysis methods are compared [Fig. 9(d)]. In both cases, the extracted cellular content was not treated/purified and was used after a delay of 20 min (handling time). We see that the gel electrophoresis of cellular DNA extracted using chemical lysis is smeared. The smeared image is attributed to the degradation of the DNA sample in the absence of treatment due to the interference of the chemicals (lysis mixture) during the time interval between lysis and GE. On the other hand, we observed a narrow band in the case of electrical lysis due to the absence and interference of any chemical, indicating effective extraction of intracellular molecules from mammalian cells, comparable to the chemical lysis method. Furthermore, the electrical lysis technique performed here is faster (within 1.0 s) than conventional chemical lysis, which takes 20 min of incubation time and does not require the addition of any reagent that could interfere with downstream analysis.

C. Continuous flow electrical lysis using the microfluidic device

The above study showed that at a minimum voltage of 100 V, the cells need to be exposed to an electric field for a duration of ~1.0 s to achieve >90% lysis efficiency, which we implemented in

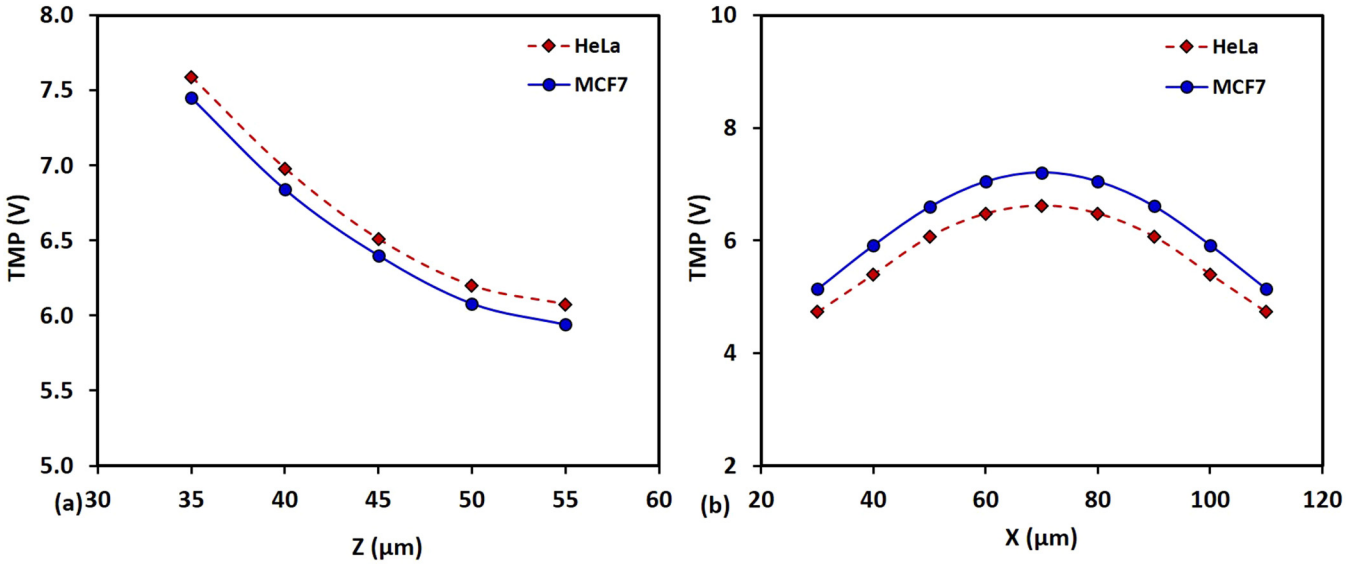

FIG. 8. Variation of TMP values from the simulations of HeLa and MCF cells with their centers placed at (a) different positions away from the electrodes along the z-direction and located at the mid-plane between the electrodes, i.e., x = 70 μm, and (b) different positions between the electrodes along the x-direction at the middle of the channel along the x-direction, i.e., z =43 μm.

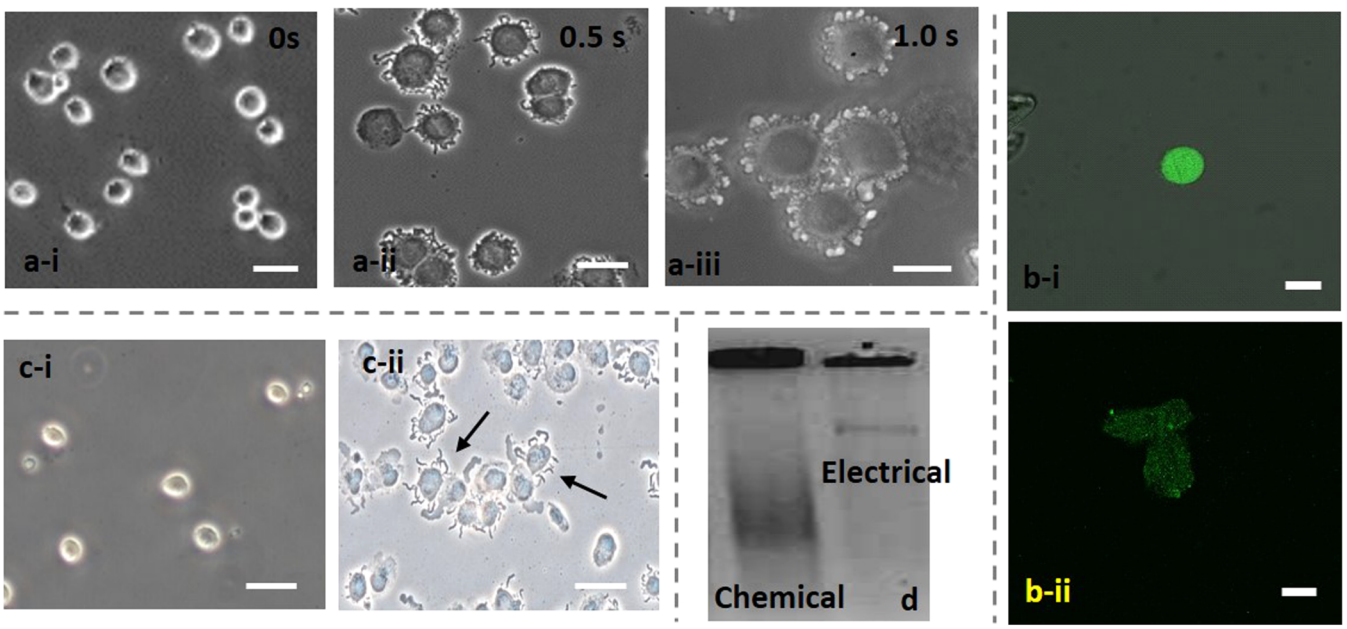

FIG. 9. The bright-field microscopic images of (a) DU 145 cells after exposing to 100 V, with the electrodes coated with PDMS of 18 μm thickness during the 1 s period (a-i) normal DU 145 cells, (a-ii) t = 0.5 s, (a-iii) t = 1.0 s, (b) comparison of a confocal microscope image of the DU 145 cells tagged with 1× Calcein AM before (b-i) and after (b-ii) electrical lysis, showing intensity degradation after cell lysis. (c) Normal DU 145 cells (i) and chemical lysis of DU 145 cells (ii), and (d) comparison of gel electrophoresis of DNA extracted using chemical and electrical lysis methods.

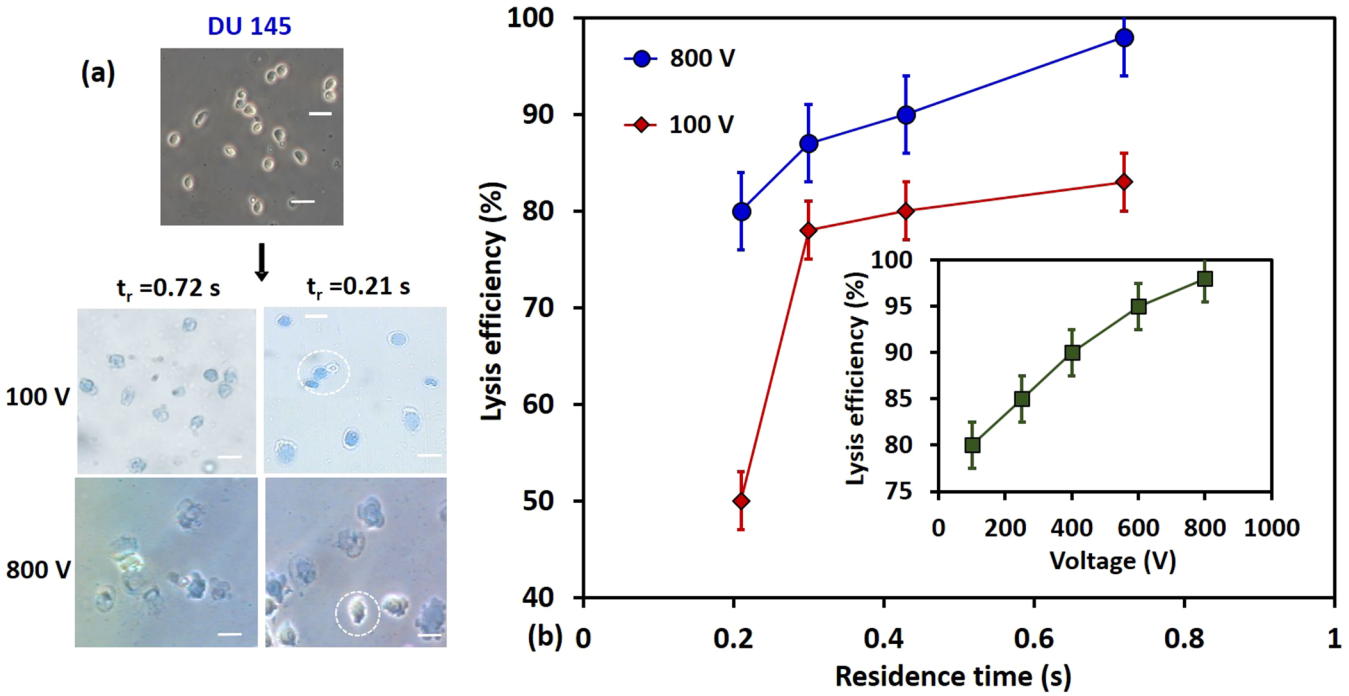

FIG. 10. (a) The bright-field microscopic images of electrical lysis of DU 145 cells at 100 V and 800 V and flow rates 0.3 and 1.0 μl/min (see video in the supplementary material). (b) The variation of lysis efficiency of DU 145 cells with voltage, 100 V and 800 V, at different flow rates; the inset shows the variation of the lysis efficiency at various applied voltage at a fixed flow rate of 0.3 μl/min.

the continuous flow microfluidic device. The effect of applied voltage and flow rate on the cell lysis efficiency was studied by varying the voltage in the range 100–800 V and the flow rate in the range 0.3 to 1.0 μl/min. At a flow rate of 0.3, 0.5, 0.7, and 1.0 μl/min, considering the channel cross section 60 × 50 μm and electrode region of width 1.2 mm, the residence times of the cells in the electrode region are 0.72 s, 0.43 s, 0.30 s, and 0.21 s, respectively. Continuous lysis of the four different cell lines (HeLa, DU 145, MDA MB 231, and MCF 7) was demonstrated and the cell lysis efficiency was obtained from the Trypan blue assay-based image analysis. The cell count in the sample at the device inlet and the number of viable vs lysed cells in the sample collected from the device outlet were obtained using a Neubauer cytometer. The microscopic images of EL of the different cells at the applied potential of 100 V and 800 V at flow rates 0.3 and 1.0 μl/min are presented in Fig. 10(a) (see video in supplementary material) and Fig. S2 in the supplementary material.

The variation of lysis efficiency of the different cells at different flow rates (0.3–1.0 μl/min) at two different voltages (100 V and 800 V) is presented in Fig. 10(b). The results show that at a fixed voltage, the lysis efficiency decreases with an increase in the flow rate, which can be due to a decrease in the residence time of cells in the high electric field region. At a higher flow rate, the cells moving faster at the center of the channel may not stay long enough in the high electric field region for the formation of irreversible pores and therefore the lysis efficiency decreases with an increase in the flow rate. The variation of lysis efficiency with the applied voltage at a fixed flow rate of 0.3 μl/min is presented in the inset of Fig. 10(b). The results show that the lysis efficiency increases with an increase in the applied voltage. Since there is a small spatial variation of the electric field and TMP in the z-direction [Fig. 8(a)], at a smaller voltage, the cells flowing far away from the channel wall have a smaller TMP and, therefore, do not get lysed resulting in a lower lysis efficiency. At higher voltages, throughout the channel cross section, the cells have higher TMP and are efficiently lysed giving a higher lysis efficiency. Furthermore, at 100 V, we observe a significant drop in the lysis efficiency when the flow rate is increased from 0.7 to 1.0 μl/min, which can be attributed to the coupled effect of a lower TMP and shorter residence time. Our results show that an applied voltage of 800 V and a flow rate of 0.3 μl/min, i.e., an electric field of 4×10^5 V/m, and residence time of 1.0 s, provide excellent lysis efficiency (~98%). Table II summarizes the lysis efficiency of the different cell lines at the maximum and minimum flow rates (0.3 μl /min and 1.0 μl /min) and voltages (100 V and 800 V) used.

The four different types of cells, HeLa, MDA MB 231, MCF 7, and DU 145 were lysed in the microfluidic device, the DNAs from the crude cell lysate were purified with Qiagen filters (Qiagen, Germany) and further analyzed and quantified using the agarose

TABLE II. Summary of the lysis efficiency and throughput of the different cell lines at maximum and minimum flow rates (0.3 μl/min and 1.0 μl/min) and voltages (100 V and 800 V) used in the experiments.

	HeLa			DU 145		
	Lysis efficiency (%)			Lysis efficiency (%)		
Voltage	0.3 μl/min	1.0 μl/min	DNA concentration (ng/μl)	0.3 μl/min	1.0 μl/min	DNA concentration (ng/μl)
100 V	83	50	41	84	56	143
800 V	98	80		98	80	
	MDA MB 231			MCF 7		
	Lysis efficiency (%)			Lysis efficiency (%)		
Voltage	0.3 μl/min	1.0 μl/min	DNA concentration (ng/μl)	0.3 μl/min	1.0 μl/min	DNA concentration (ng/μl)
100 V	80	55	133	87	60	141
800 V	98	85		98	89	

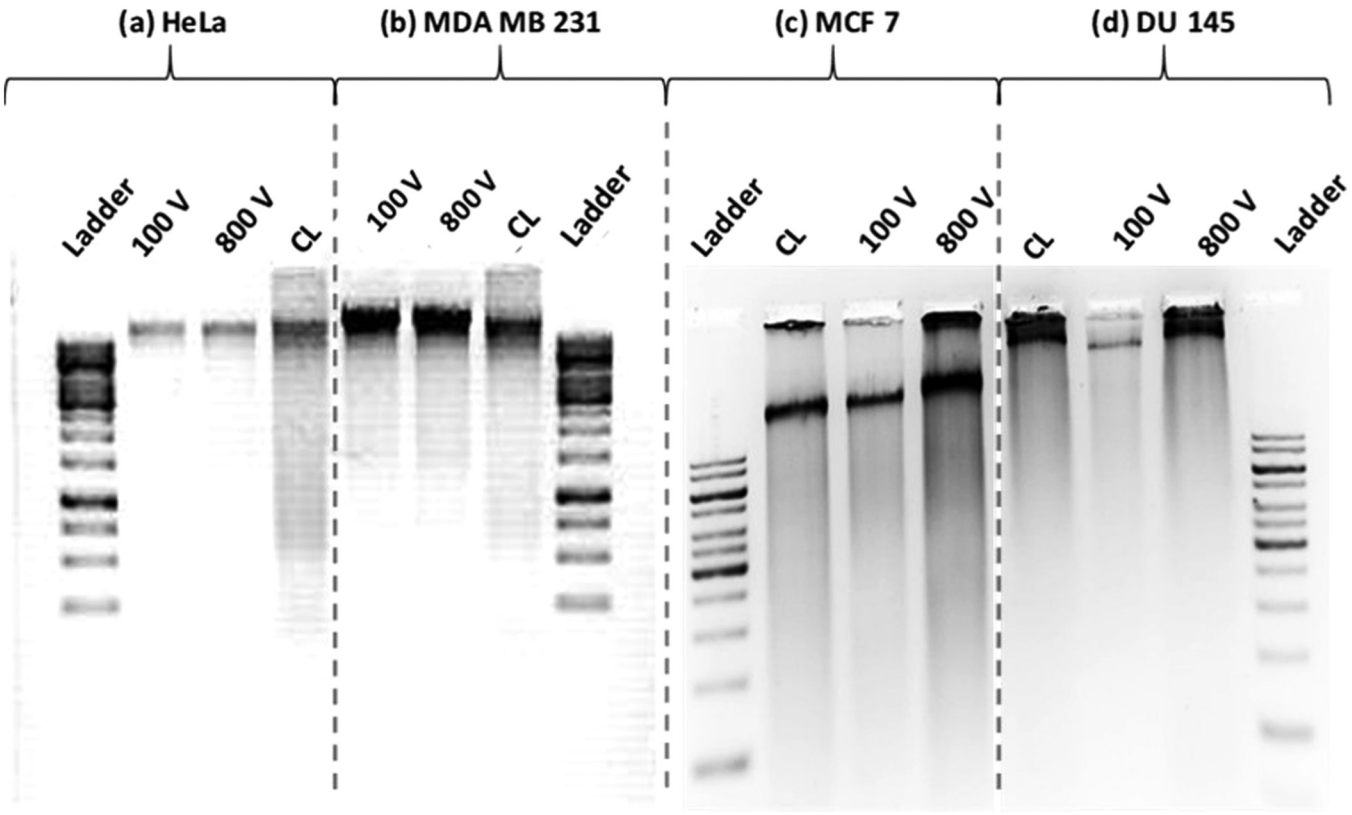

FIG. 11. Gel electrophoresis (GE) images of DNA extracted from (a) HeLa, (b) MDA MB 231, (c) MCF 7, and (d) DU 145 cells after electrical cell lysis using the microfluidic device at an applied potential of 800 V and flow rates 0.3 μl/min, for each type of cells; comparison with cell lysis using the chemical lysis method is also presented. The above images in (a)–(d) were obtained using four separate GE experiments.

gel electrophoresis (GE) method (Fig. 11). The GE images of the DNAs obtained from EL are compared with the GE image obtained from the conventional enzymatic chemical lysis (control) and the standard ladder (1Kb Gene ruler Ladder). The concentrations of the extracted DNAs were determined by comparing with the standard graphs using ImageJ software and the final concentrations were measured approximately as 41 ng/μl for HeLa, 133 ng/μl for MDA MB 231, 141 ng/μl for MCF 7, and 143 ng/μl for DU 145 cells. The DNA concentrations obtained from the GE method for the different cell lines are presented in Table II.

V. CONCLUSIONS

Herein, we reported continuous electrical lysis (EL) of four different cancer cell lines in a microfluidic device integrated with an array of passivated interdigitated electrodes. By passivating the electrodes with a thin layer (~18 μm) of PDMS, we were able to avoid two important problems that occur during EL: bubble formation (electrolysis) and electrode erosion. We carried out numerical simulations to predict the transmembrane potential (TMP) and ensure that TMP is above the critical value (~1.0 V) required for efficient EL. Our simulation results predicted that the PDMS passivation layer gives rise to a uniform electric field in the electrode region and provides a TMP in the range of 5–7 V at an applied voltage of 800 V, which is well above the critical TMP (~1 V) required for EL. The effect of the flow rate and voltage on the cell lysis efficiency was studied, which showed that the cell lysis efficiency decreases with an increase in the flow rate and decrease in the voltage, which was explained in terms of the residence time and depth-wise variation of TMP, respectively. The EL was verified using microscope imaging of cells that showed membrane protrusion and cell enlargement, live and dead cell assays, and confocal imaging. Comparison of gel electrophoresis results of DNA extracted using electrical and chemical cell lysis (CL) showed clear advantages of electrical lysis in terms of speed (~seconds in EL vs >20 min for CL) and stability of the extracted DNA due to the absence of lysis chemicals that may adversely affect downstream analysis. Using the device for continuous EL of cells at 800 V (electric field 4×10^5 V/m) and a flow rate of 0.3 μl/min (residence time of ~1.0 s), the lysis efficiency is found to be 98%. The extracted DNAs were analyzed using agarose gel electrophoresis that showed efficient recovery of genomic DNA, indicating the suitability of the EL method for downstream analysis. The EL method proposed here has great potential in the development of on-chip for ultrasensitive genetic analysis.

SUPPLEMENTARY MATERIAL

See the supplementary material for device fabrication and bright-field microscopic images of EL of different cells, and a video of the on-chip cell lysis.

AUTHORS' CONTRIBUTIONS

K.P. and P.A. contributed equally.

K.P., P.A., and A.S. fabricated devices and performed experiments. S.Z.H. carried out numerical simulations. All the authors analyzed data and wrote the manuscript. A.K.S. supervised the research.

ACKNOWLEDGMENTS

A.K.S. thanks DST and BDTD for providing financial support for the project titled "Isolation and genomic characterization of circulating tumor cells using a microfluidic platform" (No. DST/BDTD/EAG/2019), which enabled this work. The support from CNNP, IIT Madras for device fabrication is acknowledged.

DATA AVILABILITY

The data that support the findings of this study are available from the corresponding author upon reasonable request.

REFERENCES

[1]C. Dusny and A. Grünberger, Curr. Opin. Biotechnol. **63**, 26 (2020).
[2]S. M. B. Nijman, Trends Cancer **6**, 454 (2020).
[3]M. Qian, D. C. Wang, H. Chen, and Y. Cheng, Semin. Cell Dev. Biol. **64**, 143 (2017).
[4]P. J. Marc, C. E. Sims, M. Bachman, G. P. Li, and N. L. Allbritton, Lab Chip **8**, 710 (2008).
[5]N. Bao and C. Lu, Appl. Phys. Lett. **92**, 214103 (2008).
[6]K. Park, D. Akin, and R. Bashir, Biomed. Microdev. **9**, 877 (2007).
[7]P. E. Vandeventer, K. M. Weigel, J. Salazar, B. Erwin, B. Irvine, R. Doebler, A. Nadim, G. A. Cangelosi, and A. Niemz, J. Clin. Microbiol. **49**, 2533 (2011).
[8]J. Reboud, Y. Bourquin, R. Wilson, G. S. Pall, M. Jiwaji, A. R. Pitt, A. Graham, A. P. Waters, and J. M. Cooper, Proc. Natl. Acad. Sci. U. S. A. **109**, 15162 (2012).
[9]R. Sharma, B. D. Dill, K. Chourey, M. Shah, N. C. Verberkmoes, and R. L. Hettich, J. Proteome Res. **11**, 6008 (2012).
[10]E. A. Schilling, A. E. Kamholz, and P. Yager, Anal. Chem. **74**, 1798 (2002).
[11]P. Marmottant and S. Hilgenfeldt, Nature **423**, 153 (2003).
[12]D. Taller, K. Richards, Z. Slouka, S. Senapati, R. Hill, D. B. Go, and H. C. Chang, Lab Chip **15**, 1656 (2015).
[13]T. S. Santra and F. G. Tseng, Micromachines **4**, 333 (2013).
[14]M. Poudineh, R. M. Mohamadi, A. Sage, L. Mahmoudian, E. H. Sargent, and S. O. Kelley, Lab Chip **14**, 1785 (2014).
[15]S. C. Bürgel, C. Escobedo, N. Haandbæk, and A. Hierlemann, Sens. Actuators B Chem. **210**, 82 (2015).
[16]S. Ma, B. D. Bryson, C. Sun, S. M. Fortune, and C. Lu, Anal. Chem. **88**, 5053 (2016).
[17]F. Jiang, J. Chen, and J. Yu, Instrum. Sci. Technol. **44**, 223 (2016).
[18]T. Geng, N. Bao, N. Sriranganathanw, L. Li, and C. Lu, Anal. Chem. **84**, 9632 (2012).
[19]M. S. Islam, A. Aryasomayajula, and P. R. Selvaganapathy, Micromachines **8**, 83 (2017).
[20]X. Yu Wei, J. Hua Li, L. Wang, and F. Yang, Biomed. Microdevices **21**, 1 (2019).
[21]B. I. Morshed, M. Shams, and T. Mussivand, Crit. Rev. Biomed. Eng. **41**, 37 (2013).
[22]H. Jeon, S. Kim, and G. Lim, Microelectron. Eng. **198**, 55 (2018).
[23]H. Lu, M. A. Schmidt, and K. F. Jensen, Lab Chip **5**, 23 (2005).
[24]C. P. Jen, T. G. Amstislavskaya, Y. H. Liu, J. H. Hsiao, and Y. H. Chen, Sensors **12**, 6967 (2012).
[25]K. Riaz, S. F. Leung, Z. Fan, and Y. K. Lee, J. Microelectromech. Syst. **26**, 910–920 (2017).
[26]G. Mernier, R. Martinez-Duarte, R. Lehal, F. Radtke, and P. Renaud, Micromachines **3**, 574 (2012).
[27]H. J. Lee, J. Kim, K. Lim, C. Cho, N. Huh, C. Ko, C. Park, J. Choi, and S. Suk, Lab Chip **10**, 626 (2010).
[28]M. Shahini and J. T. W. Yeow, Nanotechnology **22**, 325705 (2011).
[29]Y. J. Lo and U. Lei, Micromachines **10**, 247 (2019).
[30]J. Jin and Z. M. Bhujwalla, Front. Oncol. **9**, 1560 (2019).

[31]C. Escobedo, S. C. Bürgel, S. Kemmerling, N. Sauter, T. Braun, and A. Hierlemann, Lab Chip **15**, 2990 (2015).
[32]F. Han, Y. Wang, C. E. Sims, M. Bachman, R. Chang, G. P. Li, and N. L. Allbritton, Anal. Chem. **75**, 3688 (2003).
[33]L. Nan, Z. Jiang, and X. Wei, Lab Chip **14**, 1060 (2014).
[34]S. Jaikla, T. Maturos, T. Pogfay, C. Neatpisarnvanit, P. Sritongkham, and A. Tuantranont, in *BMEiCON 2012: 5th 2012 Biomedical Engineering International Conference* (IEEE, 2012), pp. 1–5.
[35]J. S. Kee, D. P. Poenar, P. Neuzil, and L. Yobas, Opt. Express **17**, 11739 (2009).
[36]M. Carmo, D. L. Fritz, J. Mergel, and D. Stolten, Int. J. Hydrogen Energy **38**, 4901 (2013).
[37]S. Trassati, J. Electroanal. Chem. **476**, 90 (1999).
[38]S. Nandhakumar, S. Parasuraman, M. M. Shanmugam, K. R. Rao, P. Chand, and B. V. Bhat, J. Pharmacol. Pharmacother. **2**, 107 (2011).
[39]K. J. Müller, V. L. Sukhorukov, and U. Zimmermann, J. Membr. Biol. **184**, 161 (2001).
[40]P. Sajeesh, S. Manasi, M. Doble, and A. K. Sen, Lab Chip **15**, 3738 (2015).
[41]G. Pucihar, T. Kotnik, B. Valič, and D. Miklavčič, Ann. Biomed. Eng. **34**, 642 (2006).
[42]V. Jayasooriya and D. Nawarathna, in *Proceedings of the 2017 COMSOL Conference* (COMSOL, 2017); available at https://www.comsol.se/paper/download/437932/logeeshan_paper.pdf
[43]M. Y. Sulaeman and R. Widita, J. Phys. Conf. Ser. **694**, 012072 (2016).
[44]M. A. Aslam, K. Riaz, M. Q. Mahmood, and M. Zubair, RSC Adv. **9**, 41518 (2019).
[45]P. Marszalek, J. J. Zielinsky, M. Fikus, and T. Y. Tsong, Biophys. J. **59**, 982 (1991).
[46]C. Lochovsky, "Trapping and Removal of Bubbles in a Microfluidic Format," MASc Thesis, (University of Toronto, 2012). pp. 1–109.
[47]D. P. Heineck, B. Sarno, S. Kim, and M. Heller, Anal. Bioanal. Chem. **412**, 3871 (2020).
[48]J. E. Mark, *Polymer Data Handbook* (Oxford Univeristy Press, 1999), pp. 29–36.
[49]M. P. Hughes, *Nanoelectromechanics in Engineering and Biology* (CRC Press, 2002).
[50]W. F. Quirós-Solano, N. Gaio, O. M. J. A. Stassen, Y. B. Arik, C. Silvestri, N. C. A. Van Engeland, A. Van der Meer, R. Passier, C. M. Sahlgren, C. V. C. Bouten, A. van den Berg, R. Dekker, and P. M. Sarro, Sci. Rep. **8**, 1 (2018).
[51]M. C. Phelan and G. Lawler, Curr. Protoc. Cytom. **00**, A.3A.1 (1997).